JACS
JOURNAL OF THE AMERICAN CHEMICAL SOCIETY
Article
pubs.acs.org/JACS

Switchable Water: Microfluidic Investigation of Liquid–Liquid Phase Separation Mediated by Carbon Dioxide

Gabriella Lestari,[†,#] Milad Abolhasani,[‡,#] Darla Bennett,[§] Preston Chase,[⊥] Axel Günther,[‡,∥] and Eugenia Kumacheva*[,†,§,∥]

[†]Department of Chemical Engineering and Applied Chemistry, University of Toronto, 200 College Street, Toronto, Ontario M5S 3E5, Canada

[‡]Department of Mechanical and Industrial Engineering, University of Toronto, 5 King's College Road, Toronto, Ontario M5S 3G8, Canada

[§]Department of Chemistry, University of Toronto, 80 Saint George Street, Toronto, Ontario M5S 3H6, Canada

[⊥]Switchable Solutions, Inc., 945 Princess Street, Kingston, Ontario K7L 3N6, Canada

[∥]Institute of Biomaterials and Biomedical Engineering, University of Toronto, 164 College Street, Toronto, Ontario M5S 3G9, Canada

Supporting Information

ABSTRACT: Increase in the ionic strength of water that is mediated by the reaction of carbon dioxide (CO_2) with nitrogenous bases is a promising approach toward phase separation in mixtures of water with organic solvents and potentially water purification. Conventional macroscale studies of this complicated process are challenging, due to its occurrence via several consecutive and concurrent steps, mass transfer limitation, and lack of control over gas–liquid interfaces. We report a new microfluidic strategy for fundamental studies of liquid–liquid phase separation mediated by CO_2 as well as screening of the efficiency of nitrogenous agents. A single set of microfluidic experiments provided qualitative and quantitative information on the kinetics and completeness of water–tetrahydrofuran phase separation, the minimum amount of CO_2 required to complete phase separation, the total CO_2 uptake, and the rate of CO_2 consumption by the liquid mixture. The efficiency of tertiary diamines with different lengths of alkyl chain was examined in a time- and labor-efficient manner and characterized with the proposed efficiency parameter. A wealth of information obtained using the MF methodology can facilitate the development of new additives for switchable solvents in green chemistry applications.

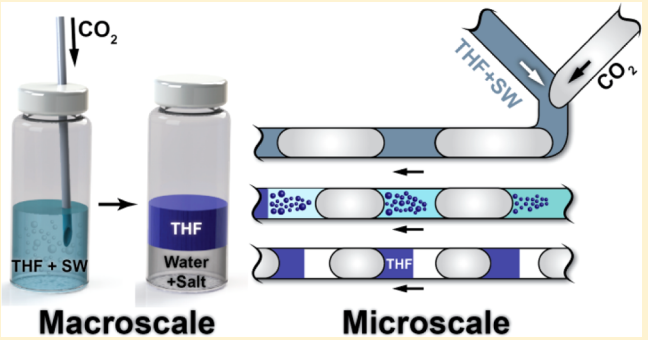

INTRODUCTION

Recently, the discovery of switchable solvents offered a promising green chemistry platform for performing consecutive chemical reactions and multistep physical processes that require different solvent properties in different stages.[1] A 'switchable' solvent is a liquid that can be reversibly changed between two states with distinct properties, such as ionic strength,[1−3] hydrophilicity,[4] polarity,[5] fluorescence,[6] or viscosity.[7,8] The liquid contains an "additive", a nitrogeneous base in the form of amine, amidine, or guanidine,[9−12] and the 'switching on' step occurs when carbon dioxide (CO_2) reacts with the base. The reaction leads to the protonation of the additive, the formation of the salt, and the change in solvent properties. To reverse these properties and recover the original liquid (to 'switch it off'), the CO_2 is removed from the liquid by heating and/or by purging an inert gas.

Since the discovery of switchable solvents by Jessop et al.,[13,14] research efforts have been largely focused on the applications of solvent switching.[3,6,15,16] In particular, CO_2 mediated increase in the ionic strength of water (water switching) had far-going implications.[3,17,18] The process of water switching is governed by the reaction (eq 1):

$$B + nH_2O + nCO_2 \rightleftharpoons BH_n^{n+} + nHCO_3^- \quad (1)$$

where B and BH_n^{n+} are the original amine and the protonated form of the amine, respectively. Increase in the ionic strength of water occurs due to the presence of ionized BH_n^{n+} and HCO_3^- products.

One of the most important applications of water switching is the desalination of water by direct (forward) osmosis.[19,20] When the ionic strength of switchable water is increased via injection of CO_2, the salt-free water is forced to move from the seawater side of the membrane (from the lower ionic strength

Received: May 5, 2014
Published: July 31, 2014

   dx.doi.org/10.1021/ja504184q | J. Am. Chem. Soc. 2014, 136, 11972−11979

water) toward the 'salty' water section. Then, the CO_2 is removed from the mixture (through heating or purging with air), the amine additive is released from the solution (in the form of gas), and the purified water becomes available.

Water switching can also lead to liquid−liquid phase separation in homogeneous mixtures of water and organic solvents via the "salting out" effect.[21] This effect is used for the recovery of water or dehydration of organic solvents and is generally achieved by adding salts, e.g., NaCl or $(NH_4)_2SO_4$ to the mixture of water and organic solvent such as acetonitrile, tetrahydrofuran, or acetone. To recover water, the salt has to be removed, which is an energy- and cost-intensive process. In contrast, switchable water (SW) can be recovered in a simple way by removing gaseous CO_2 from the solution. Furthermore, phase separation induced by water switching is important in multistep reactions, in particular, for the synthesis and functionalization of nanoparticles. Phase separation in the homogeneous mixture of water and organic solvent can lead to the mild transfer of particles into one of the phases, thereby eliminating the need of the drying step and precluding their potentially irreversible nanoparticle aggregation.[22,23]

While liquid−liquid phase separation mediated by water switching offers a promising alternative to conventional 'salting out' strategies,[24] it does not provide the efficiency of phase separation achieved by addition of conventional salts.[2] For example, addition of $(NH_4)_2SO_4$ enabled the separation of ∼99% of tetrahydrofuran (THF) from the THF−water mixture, while in the presence of *N,N,N′,N′*-tetramethyl-1,4-butanediamine, only ∼82% of THF was recovered.[2] The need in increasing the efficiency of liquid−liquid phase separation mediated by water switching necessitates a comprehensive study of this process as well as the screening of the efficiency of different nitrogenous bases. Fundamental studies and comparison of a broad range of available amine additives in a high-throughput manner would enable the optimization of the formulation used for water switching.

Figure 1a illustrates a schematic of conventional macroscale (batch) liquid−liquid phase separation experiments. A gaseous CO_2 is introduced in the form of bubbles through a needle tip into a solution of THF, water, and nitrogenous base. Later in the text, the mixture of water and the base (amine) is referred to as SW. Following reaction 1 the ionic strength of SW increases, resulting in immiscibility of THF and water, and the system phase separates into THF and an aqueous solution of the protonated form of the amine. On the macroscale, the process illustrated in Figure 1a is mass transfer limited, which implies that the measured rates of phase separation and of the reaction of CO_2 with the base depend on the reactor shape and size, the degree of mixing between the liquid and CO_2, and the method by which CO_2 is supplied to the system. Another drawback of the macroscale studies is associated with the poorly defined gas−liquid interface, due to a broad distribution of CO_2 bubble sizes. Furthermore, the process of phase separation includes several consecutive and concurrent processes: the dissolution of CO_2, the reaction of CO_2 with the base, the increase in the ionic strength of the solution, the appearance of THF droplets and droplet coalescence. Typically, samples of two liquid phases are analyzed at the beginning and the end of the experiment, while real-time characterization of the phase separation process can enable better understanding of its underlying mechanisms and kinetics of different processes.

Owing to the limitations of macroscale experiments, the following important questions remain open: What is the minimum amount of CO_2 required to complete liquid−liquid phase separation? What is the relationship between the kinetics of CO_2 consumption by the liquid medium and the kinetics of phase separation? What is the effect of amine concentration on the kinetics of phase separation process?

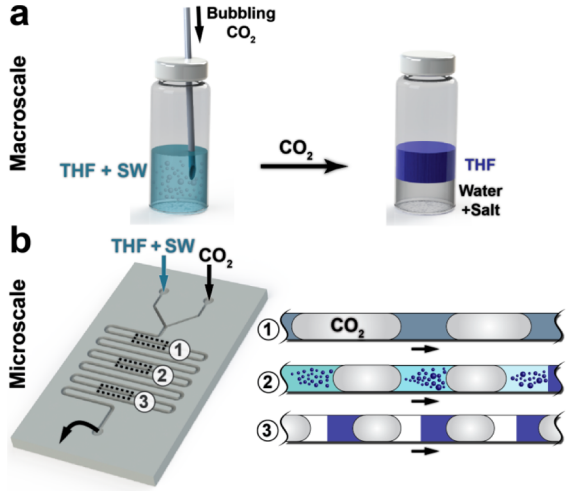

Figure 1. Phase separation of the THF−SW mixture mediated by water switching occurring on a macroscale (a) and in a MF reactor (b). Positions 1, 2, and 3 in the MF reactor (b, left) correspond to the schematics shown in (b, right): (1) generation of gaseous CO_2 bubbles (plugs) separated with segments of the THF−SW solution; (2) shrinkage of CO_2 plugs and appearance of THF droplets (dark color) in the aqueous solution of the bicarbonate salt and protonated amine (light color); and (3) coalescence of THF droplets and formation of two distinct liquid phases.

Over the past decade, microfluidic (MF) platforms have been introduced as an efficient exploratory tool for the characterization of gas−liquid processes.[25−31] Experiments were conducted using segmented flow of uniformly sized bubbles separated with liquid segments, which led to reduced axial dispersion and provided control over mass transfer time, volume fractions occupied by gases and liquids, and gas−liquid interfaces.[27,30,32] With regard to the CO_2 related processes, MFs were used for the characterization of CO_2 dissolution and solubility in physical solvents,[30,33−36] studies of reaction kinetics and thermodynamics,[27,37] and even materials science.[36,38−43] Yet, a MF strategy has not been used to study processes governed by CO_2 reactions, such as water switching and liquid−liquid phase separation.

In the present paper, we report a MF approach to fundamental studies of liquid−liquid phase separation mediated by water switching as well a screening of the efficiency of various nitrogenous bases. We show that a single set of MF experiments provides a wealth of qualitative and quantitative information on the kinetics and completeness of phase separation, the minimum amount of CO_2 required to complete phase separation, the total CO_2 consumption, and the rate of CO_2 uptake by THF−SW mixture. We demonstrate that MF experiments can be used for the time- and labor-efficient screening of the efficiency of nitrogenous agents (tertiary diamines) with varying lengths of alkyl chain in the THF−SW phase separation process and introduce an efficiency parameter to evaluate amine performance.

dx.doi.org/10.1021/ja504184q | J. Am. Chem. Soc. 2014, 136, 11972−11979

EXPERIMENTAL SECTION

Figure 1b illustrates a MF approach to studies of CO_2-mediated liquid−liquid phase separation, using THF as an exemplary organic solvent. A CO_2 gas and a solution containing a mixture of THF and SW are supplied via two inlets to the MF reactor (Figure 1b, left). When the liquid and the gaseous CO_2 streams meet at the Y-junction, the gaseous stream periodically breaks up into bubbles (plugs) separated with liquid segments (Position 1, Figure 1b (left and right)).

In the downstream channel, the CO_2 is transferred from the gaseous plugs into adjacent liquid segments, which leads to several concurrent processes: the reduction in plug volume, the reaction of CO_2 with a nitrogeneous base (Reaction 1), and an increase in ionic strength of water, causing THF−SW phase separation in the form of small THF droplets, which undergo coalescence (Position 2). In Position 3, phase separation is complete. Owing to the coalescence of the THF droplets, two distinct liquid segments, THF and an aqueous solution of the protonated base, are formed between the shrunken CO_2 plugs.

We used a glass MF reactor (the dimensions are provided in Supporting Information, section S1). The injection rates of the THF−SW mixture and the gaseous stream of CO_2 were controlled by two digital servo pressure controllers operated within the pressure range of 115−120 kPa with a resolution of 170 Pa. An inverted microscope (Olympus IX71), coupled to a CCD camera (Photometrics Cool Snap ES), was used for the optical studies of the CO_2 uptake and THF−SW phase separation process. An image analysis program (ImagePro) was used to obtain a sequence of bright-field images of the segmented gas−liquid flow at a defined resolution and frame rate. A custom-developed MATLAB image processing code was used to analyze the acquired images and extract the length and velocity of CO_2 plugs, the average intensity of the aqueous phase, and the length of the liquid segments at different positions along the MF reactor. Each set of experiments was conducted three times, with 100 images acquired for each trial. The experiments were conducted at (23 ± 1) °C.

In the first series of experiments, a tertiary diamine *N,N,N′,N′*-tetramethyl-1,4-butanediamine (TMDAB) with four carbon atoms in the alkyl chain (n = 4) was used as a nitrogeneous agent. In the second set of experiments, the efficiency of two tertiary diamines namely, *N,N,N′,N′*-tetramethyl-ethylenediamine (n = 2) and *N,N,N′,N′*-tetramethyl-1,6-hexanediamine (n = 6) was examined and compared with that of TMDAB.

Figure 2a shows a schematic of the CO_2 plugs traveling from the Y-junction in the downstream channel. The dimensions of plugs are characterized by the initial volume V_0, a reduced time-dependent volume $V(t)$, and an equilibrium volume V_f. The liquid segments separating CO_2 plugs have a volume V_S. Initially (top channel), liquid segments contain a homogeneous mixture of THF and SW. In the equilibrium state of the system (Figure 2a, bottom), the liquid segments contain a THF phase with the volume V_{THF} and an aqueous solution of the bicarbonate salt and protonated amine (a small amount of unseparated THF may remain in the aqueous solution).

We determined the following characteristics of THF−SW phase separation mediated by water switching:

Kinetics of THF−SW Phase Separation. The rate of the phase separation process was characterized by a colorimetric method. Prior to THF and SW mixing, a dye Sudan Black B was introduced in THF at the concentration of 0.1 wt %. Importantly, the dye was only soluble in THF and not in water.[44] As the THF−SW phase separation progressed, dark dye-labeled THF droplets appeared in the liquid segments, while the remaining THF−SW solution became progressively lighter, due to the reduced concentration of the dye. To monitor the change in dye intensity, $I(t)$, of the THF−SW solution over the course of phase separation, a sequence of grayscale images was analyzed by measuring the average pixel intensity of the background (see Supporting Information, section S2) corresponding to this phase.

The decay in normalized grayscale intensity $I^*(t)$ was determined as a function of time as

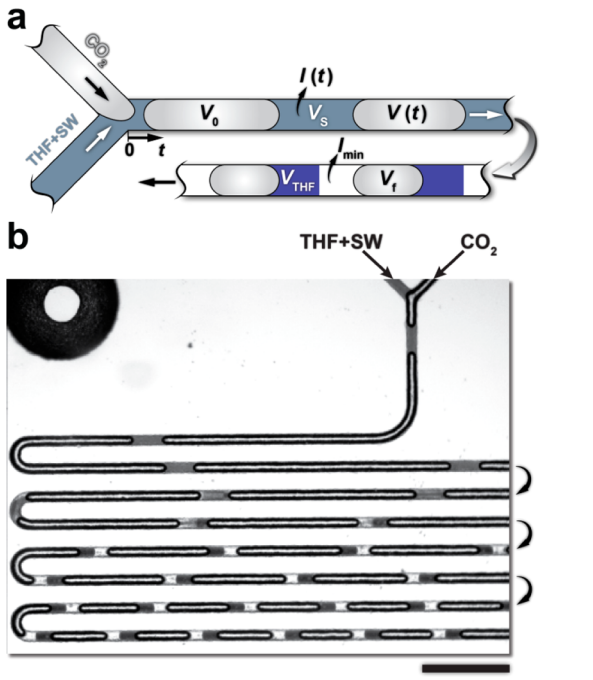

Figure 2. (a) Schematic of the initial (top) and the final (bottom) stages of the phase separation process mediated by water switching, along with measured experimental variables. (b) A typical bright-field image of gaseous CO_2 plugs and liquid segments. Polydispersities of CO_2 plugs and liquid segments are 5% and 6.2%, respectively. As time progresses, three processes are optically monitored: (1) the reduction in the length of CO_2 plugs; (2) the appearance and subsequent coalescence of dye-labeled darkTHF droplets; and (3) the reduction in color intensity of the remaining THF−SW solution in the liquid segments. Scale bar is 1 mm.

$$I^*(t) = \frac{I(t) - I_{min}}{I_0 - I_{min}} \tag{2}$$

and used to characterize the rate of change in the composition of the THF−SW solution and thus the kinetics of phase separation. In eq 2, I_0 is the average grayscale intensity of the first liquid segment after the Y-junction (taken as the baseline) and I_{min} is the minimum equilibrium intensity value, which determined the completion of phase separation.[45] A characteristic phase-separation time scale, t_S, was defined as the time required to reach 95% of I_{min}.

Efficiency of Phase Separation. The efficiency of THF−SW phase separation, η, was determined as

$$\eta = \frac{\varphi_f}{\varphi_0} = \frac{V_{THF}/V_S}{\varphi_0} \tag{3}$$

where φ_0 is the volume fraction of THF in the THF−SW solution supplied to the MF reactor, and V_{THF} and φ_f are the measured volume and volume fraction of phase-separated THF in the liquid segments after the system reached an equilibrium in the MF reactor (Figure 2a, bottom row). The volumes of the dye and the amine varying from 1.6 to 3.2 vol % were neglected.

Consumption of CO_2. To characterize the rate of consumption of CO_2 in the course of water switching and THF−SW phase separation, we determined the time-dependent number of moles of CO_2, $nCO_{2,l}(t)$, transferred to the liquid segments as

$$nCO_{2,l}(t) = \frac{P(t)\Delta V_{pc}(t)}{RT} \tag{4}$$

where $P(t)$ is the pressure in the CO_2 plug at time t along the direction of flow, ΔV_{pc} is the CO_2 plug shrinkage, due to the physical dissolution in the adjacent liquid segments and chemical reaction 1, R is gas

dx.doi.org/10.1021/ja504184q | J. Am. Chem. Soc. 2014, 136, 11972−11979

constant, and T is the temperature. Expansion of CO_2 plugs due to the pressure drop along the microchannel resulted in <5% change of CO_2 plug volume along the microchannel (Supporting Information, Section S2), The time-dependent molar concentration of CO_2 in the adjacent liquid segment, $[C_l\ (t)]$, determined by the physical dissolution and chemical consumption of CO_2, was calculated as

$$[C_l(t)] = \frac{nCO_{2,l}(t)}{V_S} \quad (5)$$

The equilibrium molar concentration of CO_2 in the liquid segment, $[C_{tot}]$, determined the total amount of CO_2 uptaken by the liquid segment in the course of phase separation. The characteristic time scale, t_e, for CO_2 mass transfer was determined as the time required to reach 95% of $[C_{tot}]$. The values of $V(t)$, ΔV_{pc}, and V_S were calculated using experimentally measured lengths of CO_2 plugs and liquid segments as described elsewhere[37] (Supporting Information, Section S2).

RESULTS

Figure 2b shows a typical bright-field optical microscopy snapshot of the processes mediated by water switching. Long, uniformly sized CO_2 plugs separated with segments of the solution containing THF, water, TMDAB, and Sudan Black B dye formed at the Y-junction of the MF reactor. The CO_2 plugs rapidly shrank, due to the transfer of CO_2 into the liquid. The volume of the liquid segments remained constant, owing to the large density difference between the gas and liquid phases (Supporting Information, Figure S3).

The transfer of CO_2 into adjacent liquid segments and its reaction with TMDAB led to water switching. This process caused THF–SW immiscibility, and resulted in the emergence of dye-labeled THF droplets in the liquid segments, accompanied by a progressive decrease in grayscale intensity $I^*(t)$ of the remaining THF–SW solution. Once the value of $I^*(t)$ reached the value of I_{min}, the phase separation process was considered to be complete. At this point, due to the coalescence of THF droplets, a distinct dye-labeled THF segment (a dark portion of the liquid segments in Figure 2b, bottom row) appeared in front of the light water segment containing a small amount of unseparated THF. The specific arrangement of water and THF segments in the microchannel is presumably governed by the wetting properties of each liquid and requires further investigation.

Figure 3a shows the decay in the normalized grayscale intensity of the THF–SW solution, $I^*(t)$, plotted as a function of time, for solutions with a varying molar concentration of amino groups, $[C_{ag}]$, of TMDAB. The value of $[C_{ag}]$ was determined as $[C_{ag}] = [C_a]f$, where $[C_a]$ is the molar concentration of amine in the THF–SW solution and f is the number of functional groups in the amine molecule ($f = 2$ for the diamines used in the present work). For the variation of I^* vs t in Figure 3a, we identified three stages of THF–SW phase separation process: (1) the initial stage, in which the increase in the ionic strength of water has not led to the notable separation of dye-labeled THF phase; (2) the linear region, in which fast THF phase separation led to the strong change in intensity; and (3) the final stage, in which phase separation reached the equilibrium state.

Several trends are explicitly shown in Figure 3a: (i) an increase in the time scale of THF–SW phase separation with decreasing $[C_{ag}]$ and (ii) a time lag, over which the change in the grayscale intensity of the THF–SW solution was below the detection limit. The lag period was ~0 and ~1 s for $[C_{ag}]$ values of 0.36 and 0.18 M, respectively. Since the CO_2–amino groups reaction started at the gas–liquid interface, we attributed a longer lag time for lower $[C_{ag}]$ to the slower replacement of the protonated amine at the interface with fresh amine molecules from the liquid segment.

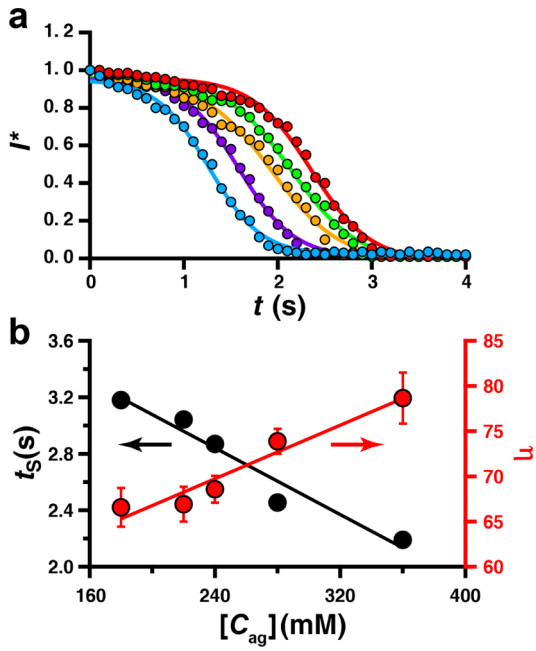

Figure 3. (a) Evolution of the normalized grayscale intensity of the THF–SW solution in the course of THF–SW phase separation. Experimental parameters: V_S= 0.015 ± 0.003 mm^3, CO_2 plug velocity is 28 ± 0.8 mm/s, φ_0 = 0.6, Sudan Black B dye:THF ratio is 1:1000 (w/w) and $[C_{ag}]$ is 0.36 M (blue circles); 0.28 M (purple circles); 0.24 M (orange circles); 0.22 M (green circle); and 0.18 M (red circle). (b) Variation in the characteristic time scale, t_S, of THF–SW phase separation (black circles) and phase separation efficiency (red circles) with varying molar concentration of amino groups. The lines are best fit (Supporting Information, section S5).

We used the linear region of the variation of I^* vs t in Figure 3a to characterize the kinetics of THF–SW phase separation at different values of $[C_{ag}]$. The rate of phase separation in this region was −1.5 (v/v) s^{-1} (Figure S4, Supporting Information) for different values of $[C_{ag}]$, indicating that the kinetics of THF–SW phase separation process was independent of amino groups concentration (Supporting Information, section S4).

Figure 3b (black circles) shows the variation in the characteristic time scale of THF–SW phase separation process, t_S, with varying $[C_{ag}]$. The highest value of t_S was obtained at the lowest value of $[C_{ag}]$, which was consistent with the corresponding longest lag time.

The efficiency of THF–SW phase separation at different values of $[C_{ag}]$ was studied by comparing the measured equilibrium volume fraction φ_f of the separated THF in liquid segments to φ_0 (eq 3). Figure 3b (red circles) shows that with increasing $[C_{ag}]$, the efficiency of TMDAB in the THF–SW phase separation, η, steadily increased. At $[C_{ag}]$ = 0.36 M, the efficiency of THF–SW phase separation was 79 ± 3%, which was comparable to 74 ± 1% obtained in macroscale experiments.[5] A small difference in the efficiency of phase separation measured in MF and macroscale experiments can be attributed to the more efficient mixing and mass transfer occurring at the microscale. We note that in Figure 3b the amount of phase separated THF did not level off, implying that $[C_{ag}]$ was not sufficiently high to reach the maximum extent of

dx.doi.org/10.1021/ja504184q | J. Am. Chem. Soc. 2014, 136, 11972–11979

THF−SW phase separation, however the utilization of higher values of $[C_{ag}]$ made the phase separation process faster than the imaging frame rate (30 frames/s) in MF experiments. This imaging limitation can be, in principle, addressed by using a high-speed camera.

Figure 4 characterizes CO_2 uptake in the process of THF−SW phase separation. With increasing $[C_{ag}]$, the time-dependent molar concentration of CO_2 in the liquid segments, $[C_l(t)]$, increased (Figure 4a). The vertical dashed lines in Figure 4a show the characteristic time scales of phase separation (obtained from Figure 3b) and indicate the minimum concentration of CO_2, $[C_{l,min}]$, required to complete THF−SW separation at corresponding values of $[C_{ag}]$. The initial rate of CO_2 consumption increased from 14.8 to 55 mM/s at $[C_{ag}]$ values of 180 and 360 mM, respectively, which was consistent with the higher THF phase separation rate at higher values of $[C_a]$ (shown in Figure 3a). After the phase separation reached an equilibrium state, the CO_2 plugs continued to shrink, presumably, to the physical dissolution of CO_2 in THF and SW segments.

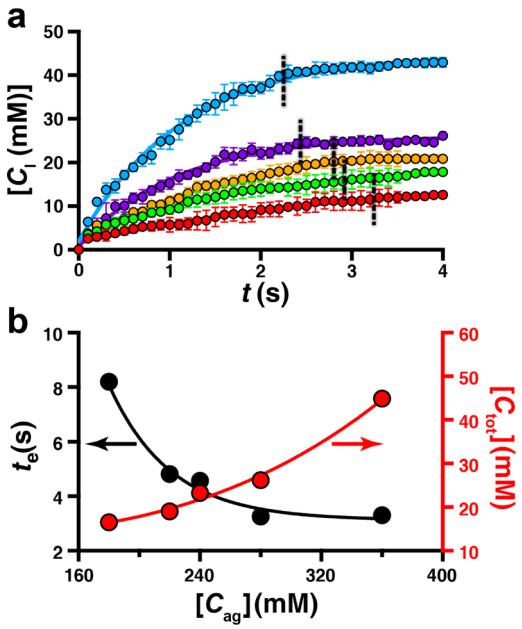

Figure 4. (a) Time evolution of CO_2 uptake by the THF−SW solution under experimental conditions used in Figure 3. (b) The total amount of CO_2 uptaken by the THF−SW solution (red circles) and the characteristic CO_2 consumption time scale, t_e (black circles), plotted for different molar concentrations of amino groups. The lines are best fit (Supporting Information, section S5).

Figure 4b (black circles) shows the effect of varying $[C_{ag}]$ of TMDAB on the characteristic time scale associated with the uptake of CO_2 by the liquid segments, t_e. Similar to the variation in t_S presented in Figure 3b, increase in $[C_{ag}]$ resulted in the reduced characteristic time scale associated with CO_2 consumption, however, the dependence of t_e vs $[C_{ag}]$ was nonlinear. In addition, Figure 4b (red circles) shows that the total amount of CO_2 uptaken by the THF−SW solution, $[C_{tot}]$, increased with increasing concentration of the tertiary amine in the mixture.

In the next set of experiments, we applied the MF approach to investigate the effect of the length of alkyl chain in diamines on THF−SW phase separation. In addition to TMDAB (n = 4), we examined two other tertiary diamines, *N,N,N′,N′*-tetramethyl ethylenediamine (n = 2) and *N,N,N′,N′*-tetramethyl-1,6-hexanediamine (n = 6). To ensure that the only parameter studied was the structure of amine, other experimental variables, including the concentration of the amino groups $[C_{ag}]$, the velocity of CO_2 plugs, the initial THF−SW volume ratio, and the volume of liquid segments V_S were maintained the same. Figure 5a shows the evolution of grayscale intensity of the aqueous phase containing different tertiary diamines. The characteristic time scale of THF−SW phase separation reduced with increasing n. The time-dependent consumption of CO_2 was the highest for TMDAB, followed by the diamines with n = 2 and 6 (Figure 5b), which indicated that this characteristic was not in direct correlation with the values of pK_{a1} and pK_{a2} of the diamines. As shown in Figure 5c, the use of *N,N,N′,N′*-tetramethyl-1,6-hexanediamine led to the highest amount of THF separated from the THF−SW mixture.

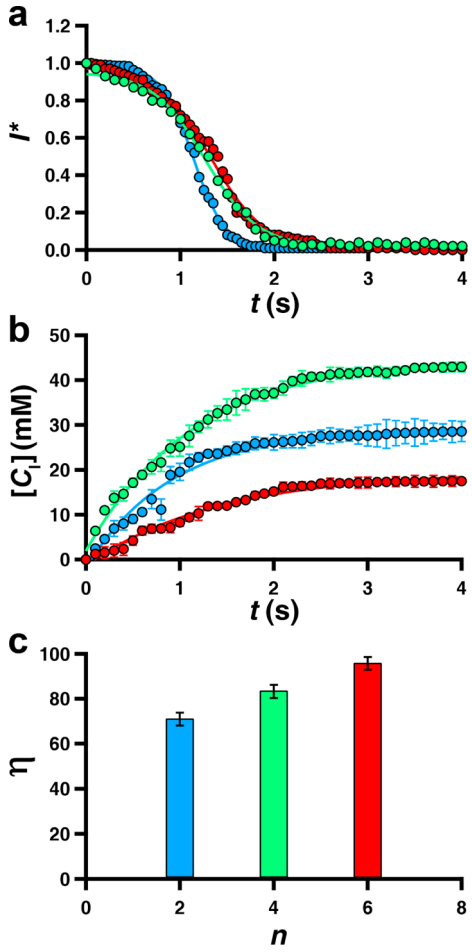

Figure 5. Effect of amine structure on the THF−SW phase separation process. The tertiary diamines used are *N,N,N′,N′*-tetramethylethylenediamine (n = 2) (blue circles); *N,N,N′,N′*-tetramethyl-1,4-diaminobutane (n = 4) (green circles); and *N, N, N′, N′*-tetramethyl-1,6-hexanediamine (n = 6) (red circles). Experimental parameters: V_S = 0.013 ± 0.002 mm^3, CO_2 plug velocity is 28 ± 0.8 mm/s, φ_0 = 0.6, Sudan Black B dye:THF ratio is 1:1000 (w/w),and $[C_{ag}]$ = 0.36 M. Time evolution of (a) grayscale intensity of the THF−SW segment and (b) CO_2 consumption by the liquid segments. (c) The efficiency of THF−SW phase separation for tertiary diamines with different lengths of alkyl chain of the nitrogeneous base.

dx.doi.org/10.1021/ja504184q | J. Am. Chem. Soc. 2014, 136, 11972−11979

DISCUSSION

The MF approach described in the present work enables simultaneous determination of a large number of characteristics of the liquid–liquid phase separation process, which are otherwise challenging or in some cases impossible to obtain using macroscale characterization techniques. This is particularly important, when several processes occur concurrently, such as CO_2 dissolution and reaction and phase separation and coalescence of phase-separated droplets.

The application of the MF strategy enabled time- and labor-efficient screening of the effect of the concentration and structure of the nitrogenous agents on the phase separation process mediated by water switching. We expect that the results obtained for the THF/SW mixture at $\varphi_0 = 0.6$ can be linearly extended to other formulations at similar THF:amine ratios (Figure S5, Supporting Information).

Moreover, the MF approach enabled comparison between the rates of the CO_2 consumption and the resulting THF–SW phase separation. Figure 6 compares the measured characteristic time scales associated with the phase separation process (t_S) and CO_2 consumption (t_e) for different concentrations of the amino groups of the nitrogenous base [C_{ag}]. As shown in Figure 6, at all concentrations of amino groups used in this study, the measured values of t_e were larger than the values of t_S, implying that an extra amount of CO_2 was always supplied into the system, not contributing to the THF–SW phase separation process. By comparing the characteristic time scales associated with the THF–SW phase separation and CO_2 consumption (indicated with dashed vertical lines in Figure 4a), we measured the minimum amount of CO_2, [$C_{l,min}$], required to complete THF–SW phase separation (Table 1). This result underlines the unique capability of MFs in studies of liquid–liquid phase separation mediated by water switching.

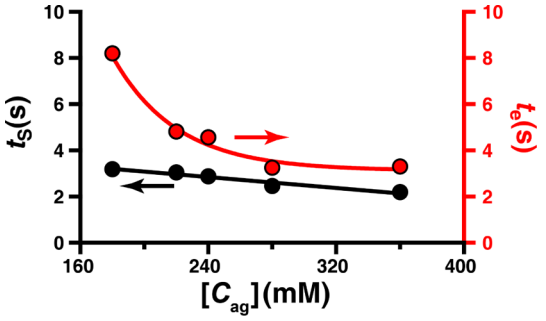

Figure 6. Comparison of the phase separation time scale (left *y*-axis, black circles) and CO_2 consumption time scale (right *y*-axis, red circles).

Importantly, the screening experiments showed that the efficiency of liquid–liquid phase separation and the minimum amount of CO_2, [$C_{l,min}$] required to achieve equilibrium phase separation do not linearly scale with the number of carbon atoms in the diamine. For example, the use of diamine with n = 6 led to the largest fraction of phase-separated THF, while the highest amount of CO_2 was consumed for the diamine with n = 4. To achieve a multicriteria decision about the efficiency of amines in the phase separation process, we propose the following rationale. The most efficient amine would lead to the highest equilibrium amount of phase-separated THF by consuming the least amount of CO_2 at the shortest t_S. Assuming a similar importance of each of these three characteristics, we introduced an efficiency parameter, E, defined as

$$E = \frac{\eta}{\left(\frac{[C_{l,min}]}{[C_{ag}]}\right)\left(\frac{t_S}{t_e}\right)} \quad (6)$$

where the numerator is the efficiency of THF–SW separation defined in eq 2, and the denominator is a product of the minimum concentration of CO_2 required to achieve THF–SW phase separation, normalized by the concentration of the amino groups, and the ratio of the characteristic time scales of THF–SW phase separation and CO_2 uptake of by the liquid segments. Based on the above definition (eq 6), the amine with a higher efficiency parameter E would be a more suitable nitrogenous agent, compared to those with lower E values.

Using eq 6, we calculated the values of E for different tertiary diamines used in the present work and ranked them in Table 1. Based on this comparison, *N*,*N*,*N*′,*N*′-tetramethyl-1,6-hexanediamine (n = 6) was the most efficient amine, compared to other diamines with a shorter length of the alkyl chain. We note that the proposed efficiency parameter is system- and application-specific, and the contribution of the characteristic parameters in eq 6 may be adjusted based on their relative importance.

CONCLUSIONS

In summary, we report a MF approach to studies of liquid–liquid phase separation mediated by water switching. In addition to strongly suppressed mass transfer limitation, good mixing, and well-defined interfaces between fluids, this method offers multiple beneficial features for studies of SW mediated liquid–liquid phase separation. Real-time *in situ* monitoring of the chemical composition of the mixture (via imaging) enables one to determine the kinetics of the phase separation process, which is impossible to obtain in macroscale systems. The *in situ* data acquisition in MF reactors enables high-throughput real-time studies of the phase separation process, which is impossible otherwise and which would facilitate the optimization of the chemical structure of the amine additives for water switching.

The MF approach offers a unique capability to explore concurrent processes such as CO_2 consumption by the liquid mixture and phase separation and compare their characteristic time scales. The wealth of information obtained from this study, including the kinetics of CO_2 uptake by the liquid mixture, the minimum amount of CO_2 required to complete phase separation, the kinetics of liquid–liquid phase separation, and the proposed efficiency parameter to screen different nitrogenous agents, will facilitate the rapid development and

Table 1. Comparison of the Performance of Tertiary Amines in THF–SW Phase Separation

n	η	[$C_{l,min}$] (mM)	[C_{tot}] (mM)	t_S (s)	t_e (s)	[C_a] (mM)	[C_{ag}] (mM)	E	ranking
6	0.96	15.1	19.5	2.18	4.28	180	360	44.3	1
2	0.71	24.1	29.0	1.65	2.66	180	360	17.1	2
4	0.83	38.6	44.9	2.20	3.35	180	360	11.8	3

dx.doi.org/10.1021/ja504184q | J. Am. Chem. Soc. 2014, 136, 11972–11979

optimization of new additives for switchable solvents. This information is of immense importance in the desalination of water, purification and separation technologies, and multistep, heterogeneous reactions occurring with transfer of products between immiscible liquid phases.

Furthermore, the developed MF strategy can be utilized for high-throughput screening of binary liquid−liquid phase diagrams at different temperatures, pressures, and compositions, thereby serving as an exploratory tool to study liquid miscibility. Moreover, the multiphase MF strategy can be extended toward other separation processes, e.g., extraction, in which comparison between characteristic time scales is of particular importance due to the high viscosity of liquids.

■ ASSOCIATED CONTENT

Supporting Information

Details of experimental setup and methods of data analysis. This material is available free of charge via the Internet at http://pubs.acs.org.

■ AUTHOR INFORMATION

Corresponding Author

ekumache@chem.utoronto.ca

Author Contributions

#These authors contributed equally.

Notes

The authors declare no competing financial interest.

■ ACKNOWLEDGMENTS

E.K. acknowledges support of NSERC Canada, Connaught Foundation and Carbon Management Canada. A.G. acknowledges support from NSERC Canada and the Ontario Research Fund (Early Researcher Award). G.L. acknowledges support from NSERC CREATE program in Microfluidic Application and Training in Cardiovascular Health (MATCH). M.A. acknowledges the Bert Wasmund Graduate Fellowship in Sustainable Energy Research and Russell A. Reynolds Graduate Fellowship in Thermodynamics. The authors acknowledge Prof. Arun Ramchandran and Prof. Philip Jessop for valuable suggestions.

■ REFERENCES

(1) Mercer, S. M.; Jessop, P. G. *ChemSusChem* **2010**, *3*, 467.
(2) Mercer, S. M.; Robert, T.; Dixon, D. V.; Chen, C. S.; Ghoshouni, Z.; Harjani, J. R.; Jahangiri, S.; Peslherbe, G. H.; Jessop, P. G. *Green Chem.* **2012**, *14*, 832.
(3) Mercer, S. M.; Robert, T.; Dixon, D. V.; Jessop, P. G. *Catal. Sci. Technol.* **2012**, *2*, 1315.
(4) Jessop, P. G.; Kozycz, L.; Rahami, Z. G.; Schoenmakers, D.; Boyd, A. R.; Wechsler, D.; Holland, A. M. *Green Chem.* **2011**, *13*, 619.
(5) Phan, L.; Andreatta, J. R.; Horvey, L. K.; Edie, C. F.; Luco, A. L.; Mirchandani, A.; Darensbourg, D. J.; Jessop, P. G. *J. Org. Chem.* **2008**, *73*, 127.
(6) Phan, L.; Brown, H.; White, J.; Hodgson, A.; Jessop, P. G. *Green Chem.* **2009**, *11*, 53.
(7) Su, X.; Cunningham, M. F.; Jessop, P. G. *Chem. Commun.* **2013**, *49*, 2655.
(8) Su, X.; Cunningham, M. F.; Jessop, P. G. *Polym. Chem.* **2014**, *5*, 940.
(9) Phan, L.; Chiu, D.; Heldebrant, D. J.; Huttenhower, H.; John, E.; Li, X. W.; Pollet, P.; Wang, R. Y.; Eckert, C. A.; Liotta, C. L.; Jessop, P. G. *Ind. Eng. Chem. Res.* **2008**, *47*, 539.
(10) Phan, L.; Chiu, D.; Heldebrant, D. J.; Huttenhower, H.; John, E. A.; Li, X.; Pollet, P.; Wang, R.; Eckert, C. A.; Liotta, C. L.; Jessop, P. G. *Ind. Eng. Chem. Res.* **2008**, *47*, 539.
(11) Wang, J. X.; Su, X.; Jessop, P. G.; Feng, Y. J. *Prog. Chem.* **2010**, *22*, 2099.
(12) Jessop, P. G.; Mercer, S. M.; Heldebrant, D. J. *Energy Environ. Sci.* **2012**, *5*, 7240.
(13) Jessop, P. G.; Heldebrant, D. J.; Li, X. W.; Eckert, C. A.; Liotta, C. L. *Nature* **2005**, *436*, 1102.
(14) Liu, Y. X.; Jessop, P. G.; Cunningham, M.; Eckert, C. A.; Liotta, C. L. *Science* **2006**, *313*, 958.
(15) Heldebrant, D. J.; Yonker, C. R.; Jessop, P. G.; Phan, L. *Chem. Eur. J.* **2009**, *15*, 7619.
(16) Holland, A.; Wechsler, D.; Patel, A.; Molloy, B. M.; Boyd, A. R.; Jessop, P. G. *Can. J. Chem.* **2012**, *90*, 805.
(17) Chen, C. S.; Lau, Y.; Mercer, S.; Robert, T.; Horton, H.; Jessop, P. *ChemSusChem* **2013**, *6*, 2.
(18) Robert, T.; Mercer, S. M.; Clark, T. J.; Mariampillai, B. E.; Champagne, P.; Cunningham, M. F.; Jessop, P. G. *Green Chem.* **2012**, *14*, 3053.
(19) Elimelech, M.; Phillip, W. A. *Science* **2011**, *333*, 712.
(20) Li, D.; Wang, H. T. *J. Mater. Chem. A* **2013**, *1*, 14049.
(21) Matkovic, Ce; Christia, Gd *Anal. Chem.* **1973**, *45*, 1915.
(22) Lohse, S. E.; Murphy, C. J. *J. Am. Chem. Soc.* **2012**, *134*, 15607.
(23) Choueiri, R. M.; Klinkova, A.; Therien-Aubin, H.; Rubinstein, M.; Kumacheva, E. *J. Am. Chem. Soc.* **2013**, *135*, 10262.
(24) Nagaosa, Y. *Anal. Chim. Acta* **1980**, *120*, 279.
(25) Kawaji, M.; Chung, P. M. Y. *Microscale Thermophys. Eng.* **2004**, *8*, 239.
(26) Kawaji, M.; Chung, P. M. Y. Proceedings of the First International Conference on Microchannels and Minichannels, Rochester, New York, April 24−25, 2003; ASME: New York, 2003; p 115.
(27) Li, W.; Liu, K.; Simms, R.; Greener, J.; Jagadeesan, D.; Pinto, S.; Gunther, A.; Kumacheva, E. *J. Am. Chem. Soc.* **2012**, *134*, 3127.
(28) Gunther, A.; Jensen, K. F. *Lab Chip* **2006**, *6*, 1487.
(29) Abolhasani, M.; Singh, M.; Kumacheva, E.; Gunther, A. *Lab Chip* **2012**, *12*, 4787.
(30) Abolhasani, M.; Singh, M.; Kumacheva, E.; Gunther, A. *Lab Chip* **2012**, *12*, 1611.
(31) Abolhasani, M.; Günther, A.; Kumacheva, E. *Angew. Chem. Int. Ed.* **2014**, *53*, 7992.
(32) Gunther, A.; Khan, S. A.; Thalmann, M.; Trachsel, F.; Jensen, K. F. *Lab Chip* **2004**, *4*, 278.
(33) Yi, C. L.; Liu, N.; Zheng, J. C.; Jiang, J. Q.; Liu, X. Y. *J. Colloid Interface Sci.* **2012**, *380*, 90.
(34) Sun, R. P.; Cubaud, T. *Lab Chip* **2011**, *11*, 2924.
(35) Lefortier, S. G. R.; Hamersma, P. J.; Bardow, A.; Kreutzer, M. T. *Lab Chip* **2012**, *12*, 3387.
(36) Tumarkin, E.; Nie, Z. H.; Park, J. I.; Abolhasani, M.; Greener, J.; Sherwood-Lollar, B.; Gunther, A.; Kumacheva, E. *Lab Chip* **2011**, *11*, 3545.
(37) Voicu, D.; Abolhasani, M.; Choueiri, R.; Lestari, G.; Seiler, C.; Menard, G.; Greener, J.; Guenther, A.; Stephan, D. W.; Kumacheva, E. *J. Am. Chem. Soc.* **2014**, *136*, 3875.
(38) Park, J. I.; Nie, Z.; Kumachev, A.; Abdelrahman, A. I.; Binks, B. R.; Stone, H. A.; Kumacheva, E. *Angew. Chem., Int. Ed.* **2009**, *48*, 5300.
(39) Park, J. I.; Nie, Z. H.; Kumachev, A.; Kumacheva, E. *Soft Matter* **2010**, *6*, 630.
(40) Park, J. I.; Tumarkin, E.; Kumacheva, E. *Macromol. Rapid Commun.* **2010**, *31*, 222.
(41) Lee, M. H.; Lee, D. *Soft Matter* **2010**, *6*, 4326.
(42) Tumarkin, E.; Il Park, J.; Nie, Z. H.; Kumacheva, E. *Chem. Commun.* **2011**, *47*, 12712.
(43) Dewick, P. M. *Essentials of organic chemistry: for students of pharmacy, medicinal chemistry and biological chemistry*; John Wiley & Sons: Hoboken, NJ, 2013.
(44) *The Sigma-Aldrich Handbook of Stains, Dyes & Indicators*; Sigma-Aldrich: Milwaukee, WI, 1990.

(45) The measured $I(t)$ of each set of experiments was normalized with respect to measured I_0 and I_{min} of the same set of experiments to remove the experimental errors associated with the light source or imaging.

dx.doi.org/10.1021/ja504184q | J. Am. Chem. Soc. 2014, 136, 11972−11979